Quantum-Mechanical Interatomic Potentials with Electron Temperature for Strong-Coupling Transition Metals

John A. Moriarty, Randolph Q. Hood, and Lin H. Yang

Phys. Rev. Lett. **108**, 036401 — Published 17 January 2012

DOI: 10.1103/PhysRevLett.108.036401

Quantum-Mechanical Interatomic Potentials with Electron Temperature for Strong Coupling Transition Metals

John A. Moriarty,* Randolph Q. Hood and Lin H. Yang

Condensed Matter and Materials Division

Lawrence Livermore National Laboratory

Livermore, CA 94551-0808

Abstract

In narrow *d*-band transition metals, electron temperature T_{el} can impact the underlying electronic structure for temperatures near and above melt, strongly coupling the ion- and electron-thermal degrees of freedom and producing T_{el}-dependent interatomic forces. Starting from the Mermin formulation of density functional theory (DFT), we have extended first-principles generalized pseudopotential theory (GPT) to finite electron temperature, and then developed efficient T_{el}-dependent *model* GPT (MGPT) interatomic potentials for a Mo prototype. Unlike potentials based on the $T_{el} = 0$ electronic structure, the T_{el}-dependent MGPT potentials yield a high-pressure Mo melt curve consistent with DFT quantum simulations as well as with dynamic experiments, and also support a rich polymorphism in the high-*T*,*P* phase diagram.

PACS: 71.15.-m, 34.20.Cf, 64.70.D-, 81.30.Bx

*Corresponding author, email: moriarty2@llnl.gov

In the past decade, high-pressure melting in transition metals [1-9] and the possibility of a solid-phase polymorphism beneath the melt curve [4,7-9] have been subjects of widespread experimental [1-3] and theoretical [4-9] interest as well as considerable controversy. The present paper focuses on two important theoretical issues that impact this and other high-temperature problems for these materials, namely, (i) the key role of *electron temperature* T_{el} near melt, especially for narrow-band 3*d* and 4*d* metals with high densities of electronic states and large observed liquid specific heats [10]; and (ii) the construction from density-functional-theory (DFT) quantum mechanics [11] of corresponding T_{el}*-dependent* interatomic potentials, which can provide up to six orders of magnitude increase in computational speed over DFT quantum simulations [5-7,9,12-14]. These potentials will allow wider investigations of structural, thermodynamic, defect and mechanical properties at high temperature, not only in high-pressure physics, but also in such diverse areas as alloy phase stability and materials design [13,14], dynamic fracture and stress corrosion cracking [15], and femtosecond laser heating [16].

As shown in Fig. 1 for bcc Mo, the effect of temperature on the DFT electronic structure near melt can be quite strong, and quantum simulations on transition metals [7,13,14] have established its importance to high-temperature structural phase stability. Although T_{el} is included in such simulations, its role is masked by the larger effect of the ion temperature T_{ion}. Here we use the Born-Oppenheimer approximation, which separates ion and electron motion and remains valid in this context, to isolate T_{el} and equilibrate the ions and electrons separately. One can thereby develop interatomic potentials for all values of T_{el}, including the limiting cases $T_{el} = 0$, which is assumed in *weak-coupling* thermodynamic models; $T_{el} = T_{ion}$, which is assumed in quantum simulations; and $T_{el} >> T_{ion}$, which occurs in ultra-fast laser experiments, where the electrons are rapidly heated before the ions can move [16]. The latter is the extreme case where melt depends strongly on T_{el}, but as we show below this is already true in metals like Mo at $T_{el} = T_{ion}$.

The supporting DFT calculations in Fig. 1 and elsewhere in this paper were performed with an accurate plane-wave pseudopotential method [12]. For Mo, a nonlocal norm-conserving pseudopotential was constructed to treat the six 5*s*, 5*p* and 4*d* valence

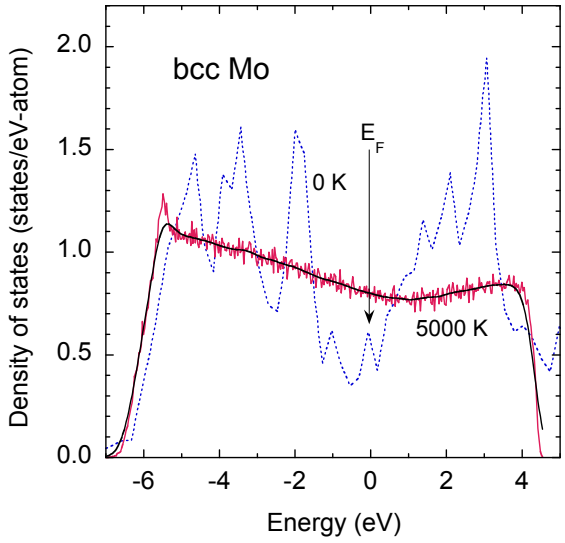

Fig. 1 Strong dependence of the electronic density of states on temperature in bcc Mo, as obtained by the present DFT quantum simulations with $T_{el} = T_{ion}$ at an atomic volume of 92.99 a.u. Result at 5000 K with smoothed solid curve represents conditions near melt.

electrons, using a plane-wave energy cutoff of 80 Ry, except for our quantum molecular dynamics (QMD) simulations of melt discussed below, where a cutoff of 60 Ry was used. Exchange and correlation were treated in the local density approximation (LDA), with generalized-gradient-approximation corrections to the LDA shown to be small for Mo.

The special importance of T_{el} in transition-metal melting was suggested two decades ago in the first quantum-based calculation of the high-pressure melt curve in Mo [17]. This calculation was performed in the conventional weak-coupling model, where the free energy A_{tot} at atomic volume Ω and temperature $T = T_{ion}$ is obtained as a sum of cold, ion-thermal and electron-thermal contributions based on the $T_{el} = 0$ electronic structure:

$$A_{tot}(\Omega, T) = E_0(\Omega) + A_{ion}(\Omega, T) + A_{el}(\Omega, T). \quad (1)$$

In this model, $A_{el} \propto \rho(E_F)T^2$, where $\rho(E_F)$ is the $T_{el} = 0$ electronic density of states (DOS) at the Fermi level E_F. The striking result obtained in Ref. 17 was that, in the absence of A_{el}, calculated melt temperatures were found to be too large by a factor of two. Lowering the Mo zero-pressure melt point close to its observed value required an

artificially large increase in $\rho(E_F)$ going from the solid to the liquid, demonstrating that A_{el} is not a small correction to A_{ion}, as is implicitly assumed in this model.

While the weak-coupling model works well in wider-band 5*d* metals such as Ta [4,18], where A_{el} is only a 5% correction in Eq. (1), this model fails in Mo due to the fact that T_{el} significantly alters the physics in this case. Because the DOS varies strongly with temperature in Mo (Fig. 1), its change upon melting is much less than calculated in the weak-coupling model. At the same time, a high T_{el} softens interatomic forces and hence the shear elastic moduli and phonons, as illustrated in Fig. 2 for C' in bcc Mo. Here C' is lowered by $15-35\%$ at melt due to T_{el} alone, with $T_{ion}=0$ in these calculations. As a result, energy barriers are lowered by T_{el} in the bcc solid, leading to lowered melt temperatures and the appearance of other competitive solid phases.

To go beyond the weak-coupling model and develop first-principles T_{el}-dependent interatomic potentials, our starting point is the finite-temperature Mermin formulation of DFT [11]. In particular, we focus on the grand potential Q_{el}, which replaces the total energy U_{tot} as the variational functional of electron density $n_{el}(\vec{r})$ in the grand canonical ensemble (constant Ω, T_{el} and chemical potential μ_{el}):

$$\begin{aligned} Q_{el} &= U_{tot} - T_{el}S_{el} - \mu_{el}N_{el} \\ &= -\int_0^\infty f_{FD}(E)N(E)dE + U_{rest} \end{aligned} \quad . \tag{2}$$

Here S_{el} is the electronic entropy, N_{el} the number of electrons, $f_{FD}(E)$ the Fermi-Dirac occupation function $\left(1+\exp[(E-\mu_{el})/k_BT]\right)^{-1}$, $N(E)$ the integrated DOS, $\int_0^E \rho(E')dE'$, and $U_{tot}=U_{band}+U_{rest}$, where U_{band} is the band-structure energy and U_{rest} contains the remaining DFT terms. The key point about the second line of Eq. (2) is that both $N(E)$ and U_{rest} are functionals of n_{el} that can be developed rigorously in multi-ion expansions. These expansions have been obtained previously for transition metals within DFT at $T_{el}=0$ via first-principles generalized pseudopotential theory (GPT) [19], using a

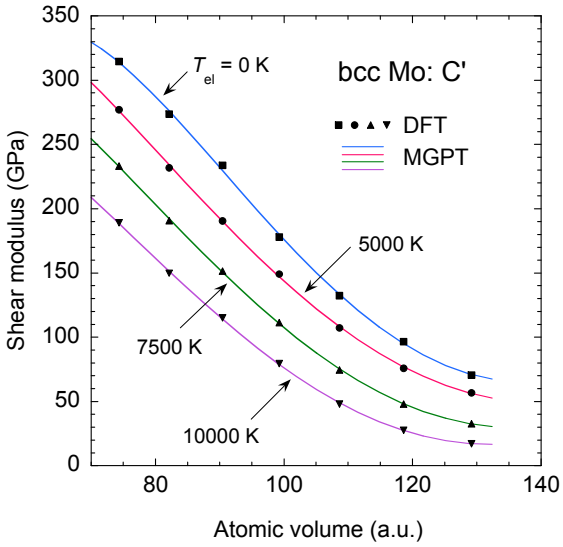

Fig. 2 Dependence of the of the shear modulus C' on electron temperature $T_{\rm el}$ in Mo, as determined from first-principles DFT calculations performed in the static bcc lattice with $T_{\rm ion} = 0$, and as used here to constrain $T_{\rm el}$-dependent MGPT potentials.

quantum-mechanical basis set of plane waves and localized, atomic-like d states. Extension of these results to finite $T_{\rm el}$ is accomplished by the insertion of $f_{\rm FD}(E)$ in the energy integrals establishing $n_{\rm el}$. The multi-ion expansions for $N(E)$ and $U_{\rm rest}$ obtained in Ref. 19 are then directly transferable to Eq. (2).

In molecular dynamics (MD) simulations, we work in the equivalent canonical ensemble (constant Ω, $T_{\rm el}$ and $N_{\rm el}$), where $Q_{\rm el}$ is replaced by the free energy $F_{\rm el} = U_{\rm tot} - T_{\rm el}S_{\rm el}$. Within the GPT, we have developed $F_{\rm el}$ as a functional of the N ion positions $\mathbf{R} \equiv \{\mathbf{R}_i\}$ in terms of $T_{\rm el}$-dependent multi-ion potentials up to four-ion interactions:

$$F_{\rm el}(\mathbf{R};\Omega,T_{\rm el}) = NF_{\rm vol}(\Omega,T_{\rm el}) + \frac{1}{2}{\sum_{i,j}}' v_2(ij;\Omega,T_{\rm el}) + \frac{1}{6}{\sum_{i,j,k}}' v_3(ijk;\Omega,T_{\rm el}) + \frac{1}{24}{\sum_{i,j,k,l}}' v_4(ijkl;\Omega,T_{\rm el}) \tag{3}$$

Here $F_{\rm vol}$ and the interatomic potentials v_2, v_3 and v_4, are structure independent and transferable to all bulk ion configurations. These quantities are explicit functionals of the *sp* pseudopotential, *d-d* tight-binding and *sp-d* hybridization matrix elements arising in

the chosen basis set. In a simulation, the force on each ion is calculated from the gradient of $F_{\rm el}$ with respect to its position. If the ions are equilibrated at temperature $T = T_{\rm ion}$, then the free energy of the system is $A_{\rm tot}(\Omega, T) = \langle F_{\rm el} \rangle - TS_{\rm ion}$, where the first term is a configuration average of $F_{\rm el}$ and $S_{\rm ion}$ is the ion entropy. This replaces Eq. (1).

Application of the full $T_{\rm el}$-dependent GPT is limited because of long-ranged *sp-d* hybridization contributions and the fact that v_3 and v_4 are non-analytic, multi-dimensional functions. To overcome this limitation, we have extended the simplified *model* GPT (MGPT) developed at $T_{\rm el} = 0$ [17,20] to finite $T_{\rm el}$, introducing approximations appropriate for nearly half-filled *d*-band metals like Mo, principally the neglect of explicit *sp-d* hybridization and the use of non-canonical *d* bands [19] to express the *d-d* tight-binding matrix elements analytically. The latter then have a simple r^{-p} radial dependence and an angular dependence quantified by the ratios $c_0 = dd\sigma / dd\delta$ and $c_1 = dd\pi / dd\delta$. Highly symmetric canonical *d* bands, which heretofore have been used in MGPT applications to Mo [17,20], are recovered in the limits $p = 2l + 1 = 5$ (for $\ell = 2$), $c_0 = 6$ and $c_1 = -4$. In the $T_{\rm el}$-dependent MGPT formalism [18], the *d*-state contributions to v_2, v_3 and v_4 are expressed as a series of five terms each involving an $\Omega, T_{\rm el}$-dependent coefficient, a single radial function $\propto r^{-p}$, and for v_3 and v_4, three angular functions, which are evaluated on the fly at each time step in the simulation by *d*-state matrix multiplication. In the case of Mo, the five coefficients together with $F_{\rm vol}$ are established by fitting $\Omega, T_{\rm el}$-dependent DFT data at $T_{\rm ion} = 0$ on the bcc equation of state, shear elastic moduli (Fig. 2), unrelaxed vacancy formation energy, and mean-squared zone-boundary phonon frequency, all up to $T_{\rm el} = 10,000$ K.

The use of non-canonical *d* bands in the case of Mo is a highly significant improvement, especially in the MGPT description of the phonons. This is due to the well-known Kohn-like anomalies in the Mo phonon spectrum, which are not adequately captured by canonical *d* bands. In this regard, for each $T_{\rm el}$ considered the parameters c_0 and c_1 were determined at a single volume (105.1 a.u.) by a least-squares fit to first-principles DFT

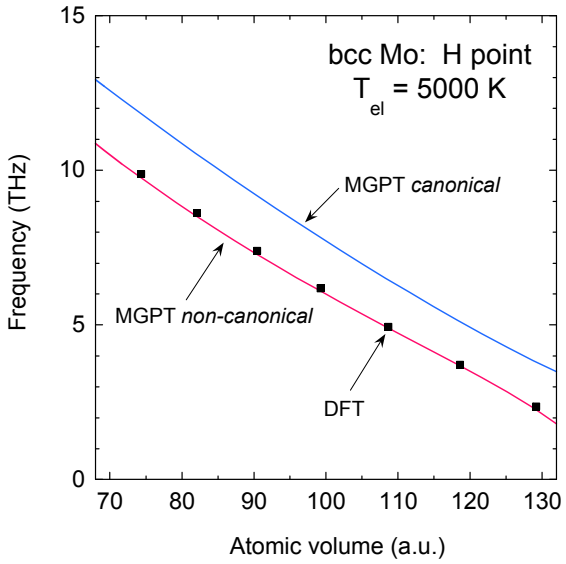

Fig. 3 Large positive impact of non-canonical *d* bands on the T_{el}-dependent MGPT calculation of the anomalous H-point phonon frequency and its volume dependence in bcc Mo at an electron temperature of 5000 K.

values of the four high-symmetry zone-boundary phonon frequencies at the H and N points in the Brillouin zone. Remarkably, the same values of c_0 and c_1 also optimize the calculated phonons at all volumes for a given T_{el}, as illustrated in Fig. 3 for the anomalous H-point phonon at 5000 K. Similar good results were obtained for the three N-point phonons at 5000 K and for the H- and N-point phonons at all T_{el}, while maintaining the observed shape of the Mo phonon spectrum [18].

We now turn to the simulation of the high-pressure melt curve in Mo as a benchmark test of the T_{el}-dependent MGPT potentials. Our central MD/MGPT and QMD results are displayed in Fig. 4 together with previous QMD melt calculations [9] and experimental melt data obtained from isobaric [10] and shock [21] measurements. The present melt results have been obtained with a robust form [18] of the standard two-phase simulation method [22], in which equilibrated solid (bcc) and liquid sub-cells are placed in contact and the motion of the solid-liquid interface monitored as a function of pressure for a trial melt temperature. The full 256-atom (solid plus liquid) computational cell used in our two-phase QMD melt simulations represented the maximum number of atoms that we

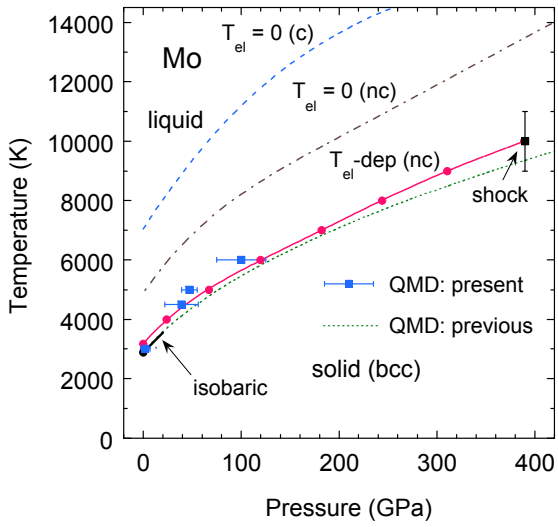

Fig. 4 High-pressure melt curve for Mo, as obtained from MD simulations with $T_{el} = 0$ and T_{el}-dependent MGPT potentials, using canonical (c) and non-canonical (nc) *d* bands, and from the present and previous (Ref. 7) QMD simulations, and as compared to experimental isobaric (Ref. 10) and shock (Ref. 21) data.

could reasonably treat for Mo. Each calculated melt point required 7-10 two-phase simulations, with a time step of 1.2 fs and a simulation time (after sub-cell equilibration) of ~ 1 ps to accumulate statistics. A total of four QMD melt points up to 100 GPa were so obtained. In contrast, cell size was not a limitation in the MD/MGPT melt simulations, and although we found no size effects beyond 256 atoms, the final T_{el}-dependent MGPT melt curve was obtained with 87,808 atoms to minimize statistical scatter in the eight calculated points up 400 GPa. We have also confirmed the weak-coupling result of Ref. 17 in the $A_{el} = 0$ limit of Eq. (1) by simulating the Mo melt curve with optimized $T_{el} = 0$ MGPT potentials based on canonical *d* bands [20]. The use of non-canonical *d* bands lowers this result, but it is still 50% too high, and only when electron temperature is included through the T_{el}-dependent MGPT potentials is the calculated melt curve brought into close proximity of the QMD and experimental data, yielding good agreement among these results. These latter results also agree with the additional DFT calculation of the Mo melt curve by Cazorla *et al*. [5].

DFT-based melt calculations in bcc Mo and Ta, including both the present results and previous calculations [4-7,9], have all produced steep *T*-*P* melt curves with increasing pressure, in general agreement with *dynamic* experimental data, but in sharp contrast to the nearly flat *T*-*P* melt curves obtained in previous *static* diamond-anvil-cell (DAC) measurements [1,2]. This has led to a decade of controversy concerning the correct interpretation of the DAC measurements, including theoretical evidence of possible solid-solid phase transitions prior to melt [4,7-9] and a recent DAC measurement of a steep *T*-*P* melt curve in Ta [3]. Using small-cell (≤ 128 atoms) QMD simulations, Belonoshko *et al.* [7] have found that the fcc structure in Mo melts at a higher temperature than bcc above ~ 150 GPa, which implies that the fcc phase is thermodynamically more stable than bcc in that regime. To explore this issue further, we have made an initial study of high *T*-*P* polymorphism in Mo using our $T_{\rm el}$-dependent MGPT potentials. We focused on a single volume corresponding to $P:$ 65 GPa at 5000 K near melt, and considered five candidate structures: bcc, fcc, fct (face-centered tetragonal, $c/a = 1.107$), hcp ($c/a = 1.633$) and hex-ω (hexagonal omega, $c/a = 0.56$). Unlike bcc, the fcc, fct, hcp and hex-ω structures are all mechanically unstable at $T = 0$ for this volume, with calculated imaginary phonon frequencies. Using MD/MGPT simulations with up to 2048 atoms, we have determined that each of the non-bcc structures is mechanically stabilized at 5000 K. This stability is driven by large anharmonic vibrational effects, which are enhanced by $T_{\rm el}$ and estimated by $Q_{\rm ah} = 100(1 - E_{\rm th}/3k_{\rm B}T)$, where $E_{\rm th} = \langle F_{\rm el} \rangle - E_0$. Here $Q_{\rm ah} = 7.4\%$ in bcc Mo at 5000 K, whereas $Q_{\rm ah}$ is 3-6 times larger in the other phases: 28.9% in fcc, 25.4% in fct, 20.8% in hcp and 43.3% in hex-ω. Once equilibrated at 5000 K, we raised the temperature in each of the five structures until melt was observed, establishing a constant-volume critical melt point T_c for each phase. We then used the Z-method of Belonoshko *et al*. [7] to estimate the thermodynamic melt temperature $T_m < T_c$. While T_m was not well established for the hcp structure by this procedure, it was for the other four candidate structures, with the final result $T_m^{\rm fcc} > T_m^{\rm fct} > T_m^{\rm bcc} > T_m^{\rm hex-\omega}$. Thus both the fcc and fct structures were found to be more stable than bcc under the assumed conditions. This supports the hypothesis that multiple solid phases, either stable or metastable, could be present in Mo under high *T*-*P* conditions.

This work was performed under the auspices of the U. S. Department of Energy by Lawrence Livermore National Laboratory under contract No. DE-AC52-07NA27344, with financial support from DOE SciDAC grant DE-FC02-06ER25788 and computing support from the LLNL Institutional Computing Grand Challenge program.

References

[1] D Errandonea *et al*., Phys. Rev. B **63**, 132104 (2001) and J. Phys. Condens. Matter **15**, 7635 (2003).

[2] D. Santamaria-Perez *et al*., J. Chem. Phys. **130**, 124509 (2009).

[3] A. Dewaele *et al*., Phys. Rev. Lett. **104**, 255701 (2010).

[4] J. A. Moriarty *et al*., J. Phys: Condens. Matter **14**, 2825 (2002).

[5] C. Cazorla *et al*., J. Chem. Phys. **126**, 194502 (2007).

[6] S. Taioli *et al*., Phys. Rev. B **75**, 214103 (2007).

[7] A. B. Belonoshko *et al*., Phys. Rev. Lett. **100**, 135701 (2008).

[8] C. J. Wu *et al.*, Nature Mater. **8**, 223 (2009).

[9] L. Burakovsky *et al*., Phys. Rev. Lett. **104**, 255702 (2010).

[10] J. W. Shaner, G. R. Gathers and C. Minichino, High Temp. High Pressures **9**, 331 (1977).

[11] N. D. Mermin, Phys. Rev. **137**, A1441 (1965).

[12] R. Q. Hood, L. H. Yang and J. A. Moriarty, Phys. Rev. B **78**, 24116 (2008).

[13] C. Asker *et al*., Phys. Rev. **77**, 220102 (2008).

[14] V. Ozolins, Phys. Rev. Lett. **102**, 065702 (2009).

[15] Chen *et al*., Phys. Rev. Lett. **104**, 155502 (2010).

[16] V. Recoules *et al.*, Phys. Rev. Lett. **96**, 055503 (2006).

[17] J. A. Moriarty, Phys. Rev. B **49**, 12431(1994) and **42**, 1609 (1990).

[18] Supplementary Notes for this paper.

[19] J. A. Moriarty, Phys. Rev. B **38**, 3199 (1988).

[20] J. A. Moriarty *et al.*, J. Mater. Res. **21**, 563 (2006).

[21] R. S. Hixson *et al.*, Phys. Rev. Lett. **62**, 637 (1989).

[22] J. R. Morris *et al*., Phys. Rev. B **49**, 3109 (1994).